Tutor

Dr. Arnald Grabulosa Rodríguez
Dept. de Química Inorgànica i Orgànica
Secció de Química Inorgànica

Grau de Química

Treball Final de Grau

Catalytic alkene and alkyne hydroacylation using Rh(I) complexes with diphosphanes

Hidroacilació catalítica d'alquens i alquins emprant complexos de Rh(I) amb difosfans

Nil Saumell Palacios

January 2024

Universitat de Barcelona

B:KC Barcelona Knowledge Campus
Campus d'Excel·lència Internacional

«...I've been driven by two passions which I acquired in graduate school: I am passionate about the Periodic Table [...], and I am passionate about catalysis.»

K. Barry Sharpless, *Nobel Lecture (2001)*

En primer lloc, vull donar gràcies als meus pares, a la meva germana i a la resta de la família per estar incondicionalment al meu costat donant-me suport. Sense vosaltres no seria on soc avui.

Als meus amics, als de sempre i als que he conegut en el grau, que han fet aquesta etapa molt més fàcil i divertida.

A tots els companys de laboratori, per la bona acollida, per tots els bons moments i pels riures, especialment a en Javier per ajudar-me sempre en tot el que he necessitat dins i fora del laboratori.

Per últim, a l'Arnald, pels consells, per tot l'entusiasme que dediques a la recerca i per ensenyar-me (i com que he vist, he cregut) com de bonica pot arribar a ser aquesta química. Moltes gràcies per ser com ets i per fer-me gaudir tant d'aquest treball.

REPORT

IDENTIFICATION AND REFLECTION ON THE SUSTAINABLE DEVELOPMENT GOALS (SDG)

Catalysis is the increase of a reaction rate and product distribution of a chemical reaction thanks to a catalyst that is not consumed in the process. Catalysis is, by definition, aligned to the sustainable development goals (SDG) since it promotes opportunities for a more sustainable production, minimizing the environmental impact of many industries.

This project is focused on homogeneous hydrogenation and hydroacylation catalysis. Both reactions allow the synthesis of products in an efficient and environmentally friendly manner, avoiding the production of chemical waste. Hydrogenation and hydroacylation have remarkable interest in chemical industries. Consequently, this project is linked to SDG 9 (Industries, Innovation, and Infrastructures), which emphasise the importance of developing sustainable industries and adopting environmentally sound industrial processes to reduce their ecological footprint.

In the same terms, this project is related to SDG 12 (Responsible Consumption and Production) which is focused on the use of cleaner and more sustainable chemical processes and reducing waste generation for a more sustainable and efficient use of resources and avoiding the air, water, and soil contamination.

CONTENTS

1. SUMMARY 3
2. RESUM 5
3. INTRODUCTION 7
3.1. Hydrogenation 7
3.1.1. Enantioselective hydrogenation 7
3.1.2. Rhodium(I) catalysts 8
3.1.3. Substrates 8
3.2. Hydroacylation 9
3.2.1. Rhodium(I)-catalyzed hydroacylation 10
3.2.1.1. *S*-based chelation control 11
3.2.2. Enantioselectivity and regioselectivity 11
3.2.3. Mechanism of intermolecular hydroacylation 12
3.3. Small bite angle diphosphane ligands 12
4. OBJECTIVES 13
5. $\mathbf{L1}$: SYNTHESIS AND COMPLEXATION 14
5.1. Synthesis and characterization of $\mathbf{L1}$ 14
5.1.1. Synthesis of $\mathbf{L1}$ 14
5.1.2. Characterization of $\mathbf{L1}$ 15
5.2. Synthesis and characterization of $\mathbf{C_1^1}$ 16
5.2.1. Synthesis of $\mathbf{C_1^1}$ 16
5.2.2. Characterization of $\mathbf{C_1^1}$ 16
5.3. Synthesis and characterization of $\mathbf{C_3^1}$, $\mathbf{C_4^1}$ and $\mathbf{C_5^1}$ 18
5.3.1. Synthesis of $\mathbf{C_5^1}$ 19
5.3.2. Characterization of $\mathbf{C_3^1}$, $\mathbf{C_4^1}$ and $\mathbf{C_5^1}$ 20
6. SYNTHESIS AND CHARACTERIZATION OF $\mathbf{C_1^0}$ 21
6.1. Synthesis of $\mathbf{C_1^0}$ 21
6.2. Characterization of $\mathbf{C_1^0}$ 21

7. FLUORENE-BASED DIPHOSPHANES 22
7.1. Synthesis and characterization of $\mathbf{L2}$ 23
7.1.1. Synthesis of $\mathbf{L2}$ 23
7.1.2. Characterization of $\mathbf{L2}$ 24
7.2. Synthesis and characterization of $\mathbf{C_1^2}$ 25
7.2.1. Synthesis of $\mathbf{C_1^2}$ 25
7.2.2. Characterization of $\mathbf{C_1^2}$ 25
7.3. Synthesis and characterization of $\mathbf{C_4^2}$ 25
7.3.1. Synthesis of $\mathbf{C_4^2}$ 26
7.3.2. Characterization of $\mathbf{C_4^2}$ 26
8. CATALYSIS 27
8.1. Enantioselective hydrogenation 27
8.2. Intermolecular hydroacylation 28
9. STERIC PROPERTIES OF $\mathbf{L1}$ 30
10. EXPERIMENTAL SECTION 31
10.1. Materials and methods 31
10.2. $\mathbf{L1}$: preparation of the ligand and its complexes 31
10.2.1. Synthesis of $\mathbf{L1}$ 31
10.2.2. Synthesis of $\mathbf{C_1^1}$ 32
10.2.3. Synthesis of $\mathbf{C_2^1}$ 32
10.2.4. Synthesis of $\mathbf{C_5^1}$ 33
10.3. Study of $\mathbf{C_1^0}$ 33
10.4. Studies of fluorene-based ligand 34
10.4.1. Synthesis of $\mathbf{L2}$ 34
10.4.2. Synthesis of $\mathbf{C_1^2}$ 34
10. CONCLUSIONS 35
11. REFERENCES AND NOTES 37
12. ACRONYMS 39

1. SUMMARY

This TFG describes the synthesis and characterization of two short-bridged diphosphanes **L1** and **L2**. Ligand **L1** is a novel chiral *P*-stereogenic methylene-bridge diphosphane that has been prepared in optically pure form. This TFG also details its complexation with rhodium(I)-diene moieties to furnish complexes $\mathbf{C_1^1}$ and $\mathbf{C_2^1}$, which have been thoroughly characterized, including the crystal structure for $\mathbf{C_1^1}$. In addition, the stable catalytic precursor $\mathbf{C_5^1}$, has been also prepared and characterized, along with other Rh(I) complexes.

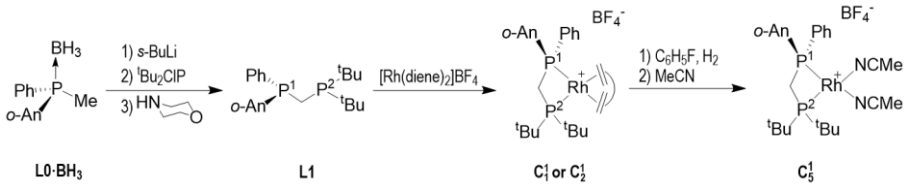

Ligand **L2** is a rigid diphosphane with a fluorene-substituted methylene bridge that has been prepared following the literature procedure. The complexation of the ligand with rhodium(I) precursors has not produced the expected complexes and the interesting species formed, which remain speculative, will be the object of further studies.

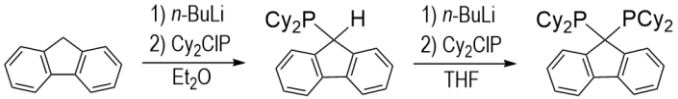

Moreover, in this TFG is described the synthesis of $\mathbf{C_1^0}$, a new bis(phosphane) complex, which has been fully characterized. Alongside with $\mathbf{C_1^1}$, these compounds have been tested as precursors in enantioselective hydrogenation, achieving high conversions, but moderate enantioselective excess.

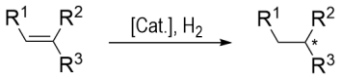

Complex $\mathbf{C_5^1}$ has been used as a catalytic precursor in intermolecular hydroacylation, furnishing good activity and selectivity results for terminal and internal unsaturated substrates.

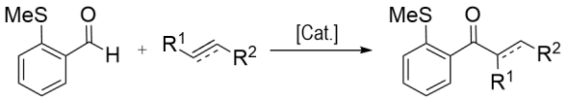

Keywords: methylene-bridged diphosphanes, *P*-stereogenic, rhodium, fluorene-based diphosphanes, enantioselective hydrogenation, hydroacylation

2. RESUM

En aquest TFG es descriu la síntesi i la caracterització de dos difosfans de pont curt, **L1** i **L2**. El lligand **L1** és un nou difosfà quiral *P*-estereogènic amb pont de metilè, que s'ha preparat de forma òpticament pura. En aquest TFG també se'n detalla la complexació de rodi(I) amb diens per formar els complexos $\mathbf{C_1^1}$ i $\mathbf{C_2^1}$, que s'han caracteritzat exhaustivament, incloent l'estructura cristal·lina de $\mathbf{C_1^1}$. També, s'ha preparat i caracteritzat el precursor catalític estable $\mathbf{C_5^1}$, juntament amb altres complexos de Rh(I).

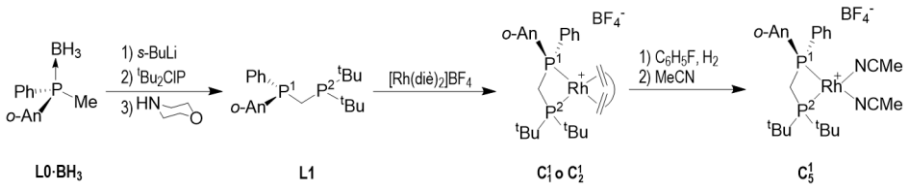

El lligand **L2** és un difosfà rígid amb el pont de metilè substituït amb un fluorè, que s'ha preparat seguint un procediment bibliogràfic. La complexació amb precursors de rodi(I) no han produït els complexos esperats, però se n'han format d'altres d'interessants, que malgrat ser especulatius, seran objecte d'estudis futurs.

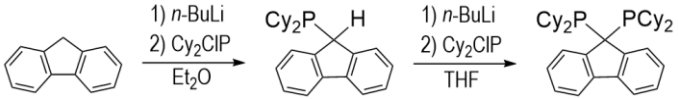

A més a més, en aquest TFG es descriu la síntesi de $\mathbf{C_1^0}$, un nou complex bis(fosfà), que també s'ha caracteritzat exhaustivament. Juntament amb $\mathbf{C_1^1}$, aquests complexos s'han provat com a precursors catalítics en hidrogenació enantioselectiva i han produït conversions elevades però amb una baixa estereoselectivitat.

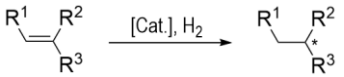

El complex $\mathbf{C_5^1}$ ha s'ha utilitzat com a precursor catalític en hidroacilació intermolecular i ha proporcionat una bona activitat i selectivitat per a substrats insaturats tant terminals com interns.

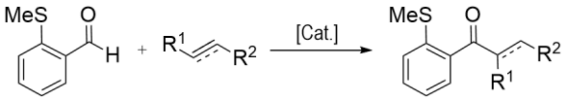

Paraules clau: difosfà amb pont de metilè, *P*-estereogènic, rodi, fluorenil difosfà, hidrogenació enantioselectiva, hidroacilació

3. INTRODUCTION

Catalysis can be defined as the increase of the reaction rate by decreasing the activation energy, facilitated by a catalyst that changes the mechanism of the reaction, but remains unconsumed. Therefore, catalysis provides a cleaner and more efficient way of production both in industry and in basic research. Classically, it is well known that catalysis is divided in two classes: heterogeneous catalysis where reagents and catalyst are in different phases and homogeneous catalysis where both are in the same phase. Heterogeneous catalysis has been heavily used in bulk chemistry, having a greater impact on industrial processes (for example in the Haber-Bosch synthesis of ammonia), while homogeneous catalysis, which has a remarkable importance in the agrochemical and pharmaceutical industries, is widely used in fine chemistry.[1]

Different classifications exist within homogeneous catalysis, with organometallic catalysis being a notable category. In this kind of catalysis, the catalyst is a metal center surrounded by organic ligands and other ancillary ligands, often an organometallic species that is soluble in the common solvents. Organometallic catalysis using transition metals has been applied to an extensive range of reactions, allowing the obtention of products with high selectivities and conversions. The properties of the catalyst are influenced by both the metal and the ligands.[1,2]

3.1. HYDROGENATION

The hydrogenation reaction is the addition of a hydrogen molecule to an unsaturated compound. One of the first and most important example of homogeneous hydrogenation catalyst was Wilkinson's catalyst, $[RhCl(PPh_3)_3]$, reported in the 1960s.[3] The d^8 configuration of the rhodium(I) atom center leads to a 16-electron square planar complex, soluble in typical organic solvents, which was shown to be able to hydrogenate olefins under mild conditions (1 bar of H_2 pressure, room temperature) catalytically.[2]

3.1.1. Enantioselective hydrogenation

The simple idea to change the achiral triphenylphosphane ligand with chiral phosphanes proved to be one of the most brilliant in the history of organometallic chemistry because thanks

to the presence of an enantiopure catalyst, catalytic enantioselective hydrogenation was born.[1] This reaction has a great interest in current chemistry since it provides enantioenriched products. The most widely used catalysts are ruthenium, rhodium, and iridium complexes.[4] In 2001 William S. Knowles and Ryoji Noyori were awarded with the Nobel Prize for their studies in this field along with K. Barry Sharpless for his research on enantioselective oxidation. Knowles and Noyori worked with diphosphane ligands, S. Knowles developed the *P*-stereogenic diphosphane **DIPAMP**,[5] and Noyori the atropoisomeric diphosphane **BINAP**[6] (Figure 1).

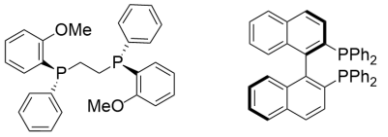

(*R,R*)-DIPAMP (*R*)-BINAP

Figure 1. Structures of (*R,R*)-DIPAMP and (*R*)-BINAP.

3.1.2. Rhodium(I) catalysts

Since the advent of enantioselective hydrogenation, extensive research has been performed on rhodium catalysts, leading to exceptionally high enantioselectivities for prochiral —substrates that can be converted in chiral products— functionalized alkenes.[4] An important type of ligands are *P*-stereogenic diphosphanes: these ligands follow the naïve idea that better enantioselective catalysts are achieved when the stereogenic atom is closer to the metal center. The experimental conditions required in catalysis are mild: low H_2 pressure, no temperature control, and low catalyst concentration. It is interesting to note that some of the best ligands in enantioselective hydrogenation are rather simple "short-bridged" diphosphanes, with a single atom (often a methylene) bridge between the phosphorus moieties (Figure 2).[4]

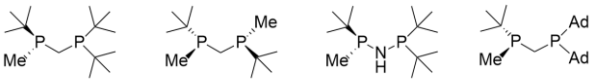

(*S*)-TCPF (*R,R*)-^{t}Bu-MiniPHOS (*S*)-MaxPHOS (*R*)-BulkyP*

Ad = adamantyl

Figure 2. Examples of highly successful short-bridged *P*-stereogenic diphosphanes for hydrogenation.

3.1.3. Substrates

Rhodium catalysts have proven their efficiency in an extensive number of functionalized substrates. The presence of a functional group, usually bearing a carbonyl moiety, is needed for the catalysis take place efficiently and with high enantioselectivity.[4] Rhodium-based catalysts

have been typically applied to five categories of substrates: α-(acylamino)acrylates **(I)**, itaconic acid derivatives **(II)**, α-alkyl- or aryl-substituted enamides **(III)**, α-alkyl- or aryl-substituted enol ester derivatives **(IV)**, and β-(acylamino)acrylates **(V)** (Figure 3).[4]

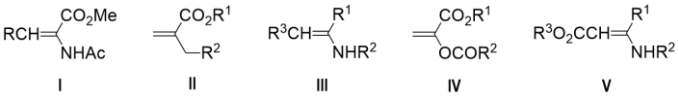

Figure 3. Benchmark functionalized olefins for enantioselective hydrogenation.

Three benchmark substrates have been used in this project, two α-(acylamino)acrylates and an itaconic acid derivate which are typical for the evaluation of catalysts. These kinds of substrates have a significant importance in the fine chemistry industry. The hydrogenation of α–(acylamino)acrylates give access to enantiopure α-amino acids.[4,7] The substrates used are (*Z*)-α-acetamidocinnamate (*Z*-MAC) (**S1**), and ethyl α-acetamidoacrylate (MAA) (**S2**). The itaconic acid derivative tested is dimethyl itaconate (DMI) (**S3**) (Figure 4).

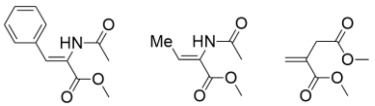

Figure 4. Benchmark substrates used in this TFG.

3.2. HYDROACYLATION

The hydroacylation reaction is the addition of an acyl group and a hydrogen atom from aldehyde across a double bond of an alkene or alkyne, to produce a ketone. In current chemistry, hydroacylation is a reaction of interest because it involves the formation of a new C–C bond in an atom-economic manner.[9] Intramolecular hydroacylation is a well-documented reaction, while its intermolecular counterpart has been much less studied, despite having a great potential due to the vast array of aldehydes and unsaturated compounds available for the reaction (Scheme 1).[9]

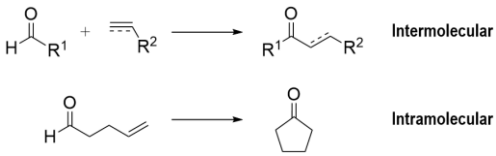

Scheme 1. Intermolecular and intramolecular hydroacylation reactions.

The first example of catalytic intramolecular hydroacylation was the synthesis of cyclopentanones reported by Sakai and coworkers in 1972, using a stoichiometric amount of

Wilkinson's catalyst.[10] A few years later Miller and co-workers reported for the first time an intermolecular hydroacylation. Studying the intramolecular reaction of 1-pentenal in a saturated solution of ethylene and changing Wilkinson's complex for [Rh(acac)(C_2H_4)$_2$], they observed the formation of a mixture of heptanones.[11]

3.2.1. Rhodium(I)-catalyzed hydroacylation

Hydroacylation reactions can be catalyzed by transition metal complexes. Intramolecular reactions are almost exclusively catalyzed with rhodium catalysts, whereas intermolecular reactions have been catalyzed by systems of other metals, including ruthenium, cobalt, iridium, and nickel. However, despite the broader range of possible metals, rhodium(I) complexes are the most used catalysts.[9,12]

Some of the best ligands for intermolecular hydroacylation are short-bridged diphosphanes, bearing a methylene bridge between the phosphorus atoms.[4] The studies have evolved from using simple ligands such as the symmetric diphosphane dppe —which only can catalyze the hydroacylation of activated alkenes— to the more complex unsymmetrical methylene bridged ligands such as **AmpaPhos**,[13] which have produced good results for terminal and, the less active, internal alkenes (Figure 5).[9,14]

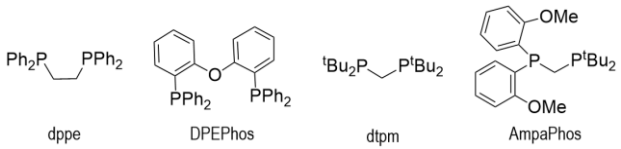

Figure 5. Some examples of diphosphane ligands used in intermolecular hydroacylation.

On the other hand, for methylene-bridged diphosphanes the catalyst needs an ancillary ligand for the catalysis to take place, being fluorobenzene one the most typically used (Figure 6).[13]

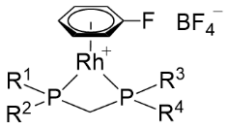

Figure 6. A typically used rhodium(I) catalytic precursor for hydroacylation.

A limitation of rhodium catalysts in intermolecular systems is the reductive decarbonylation of the acyl-metal hydride intermediate during the catalysis (Scheme 2). This pathway poisons the catalyst and reduces the activity of the catalytic systems.[13]

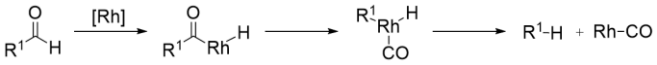

Scheme 2. Reductive decarbonylation process.

To attenuate the reductive decarbonylation of the catalyst, chelation control has been proven as an effective strategy. This method is based on the coordination of a heteroatom to the metal center during the catalysis to stabilize the key acylrhodium intermediate. N-, P-, O-, and S-based chelation control have been studied. In most of the reported examples, the aldehyde bears the heteroatom that coordinates to the metal.[9,15]

3.2.1.1. S-based chelation control

Willis, Weller, and co-workers[15] have developed the β-S-based chelation applied to intermolecular hydroacylation reactions. This method was tested with α-, β- and γ-methyltioaldehydes under the same reaction conditions, and the results show that the β position provides lower rates of decarbonylation, due to the stabilization provided by the formation of a five-membered acylrhodium intermediates (Scheme 3).[9]

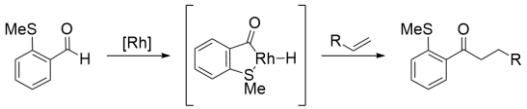

Scheme 3. Example of intermolecular hydroacylation using β-S-chelation control.

3.2.2. Enantioselectivity and regioselectivity

Intermolecular enantioselective hydroacylation is an underdeveloped field and the reported examples are limited due to the low reactivity of internal alkene and alkynes in this kind of reaction. More recently, new rhodium(ı) complexes with methylene-bridged diphosphane have been reported as promising catalysts for the activation of internal alkenes.[17] The two main challenges to develop asymmetric hydroacylation are the synthesis of a selective chiral catalyst and the correct selection of aldehyde and alkene or alkyne combination.[17]

If enantioselectivity is not considered, two products can be obtained based on the regioselectivity. Depending on which unsaturated carbon the hydride insertion occurs the linear or the branched products can be obtained (Scheme 4). Generally, in alkynes, the formation of the linear product is favoured due to the lower energy barrier of the hydride insertion and the faster reductive elimination. Nevertheless, the synthesis of ligands to achieve branched selectivity is an interesting topic of study since it can provide chiral products. [9,17]

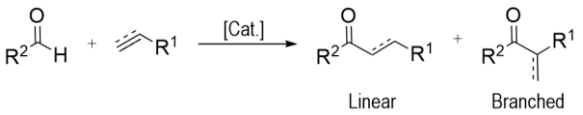

Scheme 4. Linear and branched hydroacylation products.

3.2.3. Mechanism of intermolecular hydroacylation

The accepted catalytic mechanism for rhodium-catalyzed intermolecular hydroacylation involves the aldehyde coordination to form a chelate (**A**), an oxidative addition of the aldehyde from Rh(I) to Rh(III), to form the key acyl hydride intermediate (**B**), alkene coordination (**C**), followed by the hydride insertion to the double bond (**D**), insertion of the alkyl into the Rh-carbonyl bond (**E**), and, finally, the reductive elimination that produces the ketone and regenerates the catalyst (Scheme 5). Reductive elimination seems to be the rate determining step of the cycle.[16]

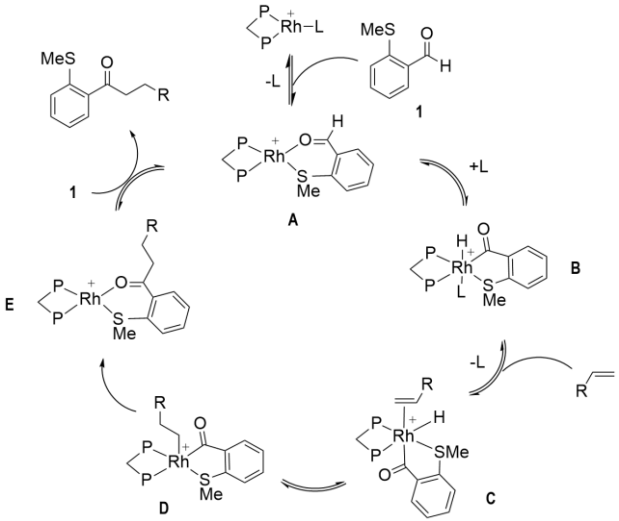

Scheme 5. Catalytic cycle for intermolecular hydroacylation with chelation-assistance.

3.3. SMALL BITE ANGLE DIPHOSPHANE LIGANDS

The bite angle is defined as the angle formed between the metal center and the two chelating atoms of a bidentate ligand. Small bite angle diphosphanes ligands have been applied in catalytic reactions such as hydrogenation or hydroacylation. Ligand bite angle is an important parameter to consider since it affects species equilibria, selectivity, rates of reductive elimination, and rates of oxidative addition. Willis, Weller, and coworkers studied the importance of the bite angle in

hydroacylation catalysis, and they concluded that although wide and narrow bite angle ligands can be used successfully, small bite enhance the reactivity of alkenes and alkynes.[9,14]

This work is focused on methylene-bridged and fluorene-based diphosphanes. Methylene-bridged diphosphanes present a $–CH_2–$ linker between the two phosphorous groups. In fluorene-based ligands, beside the substituents effect, the bridge is the quaternary carbon of the fluorene which provides more rigidity to the structure. The disubstitution of the methylene bridge would cause a Thorpe-Ingold effect, leading to the compression of the P–C–P angle, which should provide better chelating ligands.[14]

The phosphane substituents affect the P–M bond, aryl and, to a greater extent, alkyl groups are σ-donors, causing an electron enrichment of the phosphorus atoms, increasing the electron density on the transition metal, and leading to stronger P–M bonds, especially with late transition metals.[14]

In this project the synthesis of the small bite-angle diphosphane ligands **L1** and **L2** is described (Figure 7), along with its complexation with different rhodium precursors. Ligand **L1** combines Willis and Weller's **AmpaPhos**,[13] and Knowles' **DIPAMP**,[5,7] with the objective of obtaining an optically pure catalyst for enantioselective intermolecular hydroacylation. Hydrogenation and hydroacylation catalysis have been performed with **L1** complexes. On the other hand, the rigidity effect of fluorene-based diphosphane, has never been studied in hydroacylation. For this reason, **L2** has been synthesized to be used in future catalytic studies.

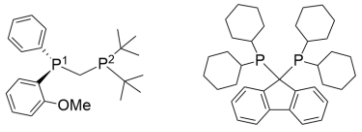

dcPAMP
L1

$Flu(PCy_2)_2$
L2

Figure 7. Ligands synthesized in this TFG.

4. OBJECTIVES

1. Synthesis of the non-symmetric, methylene-bridged, *P*-stereogenic diphosphane **L1** and the achiral fluorene-based diphosphane **L2**.

2. Study the complexation of **L1** and **L2** with rhodium(I) precursors.
3. Study the performance of the obtained rhodium(I) complexes in enantioselective hydrogenation of functionalized olefins and in alkene and alkyne intermolecular hydroacylation.

5. L1: SYNTHESIS AND COMPLEXATION

Ligand **L1** is a non-symmetric *P*-stereogenic diphosphane ligand, that was synthesized following previous work of Homogeneous Catalysis group at the University of Barcelona.[19,20] The preparation of the catalyst, starts with synthesis of the ligand **L1**, followed by its complexation, which has been done with two different rhodium(I) precursors (cod and nbd) to form $\mathbf{C_1^1}$ and $\mathbf{C_2^1}$ and, finally, the hydrogenation of the precursor diene and coordination of the labile fluorobenzene, to form $\mathbf{C_3^1}$ (Scheme 6).

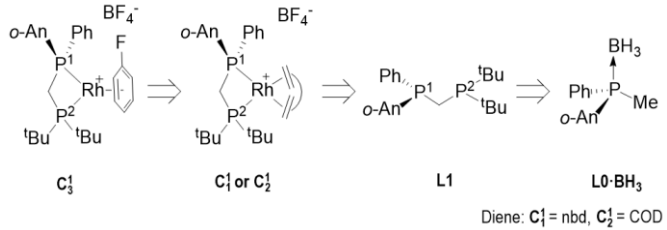

Scheme 6. Retrosynthetic analysis of $\mathbf{C_3^1}$.

5.1. SYNTHESIS AND CHARACTERIZATION OF L1

5.1.1. Synthesis of L1

The synthesis of **L1** begins with the preparation boronated **PAMP** ($\mathbf{L0 \cdot BH_3}$), which was previously synthesised following the Jugé-Stephan method (Scheme 7).[18]

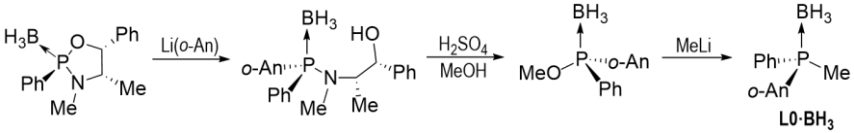

Scheme 7. Synthesis of $\mathbf{L0 \cdot BH_3}$.

As detailed in Scheme 8, a solution of $\mathbf{L0 \cdot BH_3}$ was cooled to −30 ºC, and the methyl group was deprotonated using *s*-BuLi. Then, the obtained product was reacted with di(*tert*-butyl)chlorophosphane. To deprotect $\mathbf{L1 \cdot BH_3}$, it was dissolved in morpholine and stirred overnight. To remove the morpholine–borane adduct and obtain the final ligand, a solution in toluene was eluted through alumina. This methodology has been used in the group for the synthesis of other *P*-stereogenic diphosphane ligands.[19,20]

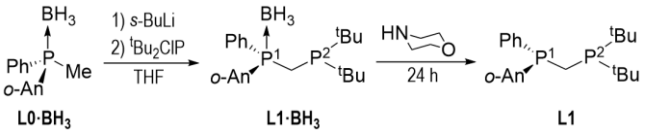

Scheme 8. Synthesis of $\boldsymbol{L1}$.

5.1.2. Characterization of L1

$\mathbf{L1}$ was characterized by ^{1}H, ^{31}P{^{1}H} and ^{13}C{^{1}H} NMR spectroscopy. These studies confirm the identity and purity of the ligand. The ^{31}P{^{1}H} NMR spectrum (Figure 8) shows two doublets at +17.5 and −23.7 ppm ($J_{P\text{-}P}$ = 142.1 Hz) corresponding to P^2 and P^1, respectively. The peaks are doublets because of the coupling between the two different phosphorus atoms, this coupling indicates the correct formation of $\mathbf{L1}$. P^2 appears at lower fields due to the steric hindrance of the two *tert*-butyl groups, while P^1 corresponds to the doublet at higher fields.

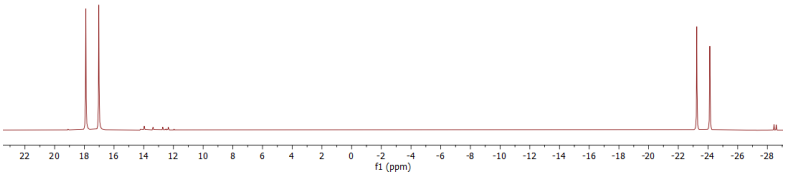

Figure 8. ^{31}P{^{1}H} NMR spectrum (162 MHz, $CDCl_3$) of $\mathbf{L1}$.

The ^{1}H NMR spectrum (Figure 9) contains a signal integrating 1H as a doublet of doublets of doublets centred at 2.24 ppm, assignable to one methylene bridge hydrogens. The geminal proton-proton coupling ($^{2}J_{H\text{-}H}$ = 14.0 Hz) and the two different couplings H–P can be seen. The other methylene bridge hydrogen appears as a doublet at 1.9 ppm ($^{2}J_{H\text{-}H}$ = 13.9 Hz), only the geminal coupling is observed. These two peaks indicate the expected reaction between $\mathbf{L0 \cdot BH_3}$ and the chlorophosphane. Two doublets that correspond to the diastereotopic *tert*-butyl groups appear at 1.10 and 0.90 ppm. In the ^{13}C{^{1}H} NMR spectrum, the methylene bridge carbon appears

at +17.4 ppm as a doublet of doublets because of a different coupling to each of the phosphorus atoms.

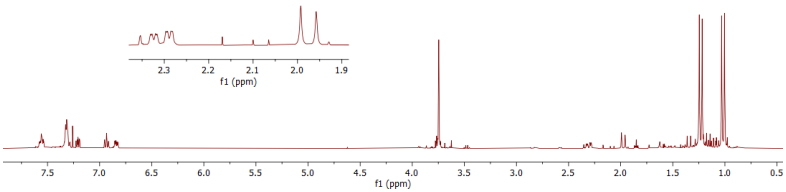

Figure 9. ^{1}H NMR spectrum (400 MHz, $CDCl_3$) of $\mathbf{L1}$, with an expansion of the methylene bridge protons.

5.2. SYNTHESIS AND CHARACTERIZATION OF $\mathbf{C_1^1}$

5.2.1. Synthesis of $\mathbf{C_1^1}$

A solution of the ligand $\mathbf{L1}$ in dichloromethane was added dropwise to another dichloromethane solution containing 0.75 equivalents of $[Rh(nbd)_2]BF_4$, to prevent the formation of the bischelated complexes (Figure 10), as observed in previous research.[19,21] The reaction mixture was stirred for 1.5 h at room temperature and a red product was obtained after evaporation of the solvent. The crude complex was recrystallized in DCM/Et_2O (Scheme 9).

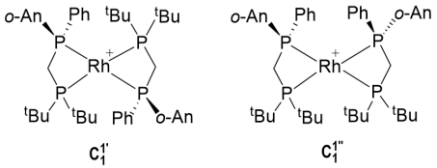

Figure 10. *Trans*- (left) and *cis*-bischelated (right) structures.

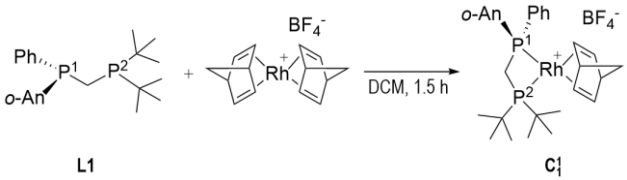

Scheme 9. Synthesis of complex $\mathbf{C_1^1}$.

5.2.2. Characterization of $\mathbf{C_1^1}$

$\mathbf{C_1^1}$ was characterized by IR spectroscopy, ^{1}H, ^{31}P{^{1}H}, ^{13}C{^{1}H} NMR spectroscopy and COSY ^{1}H–^{1}H and HSQC ^{1}H–^{13}C 2D NMR spectroscopy. Also, the crystal structure could be obtained by X-ray diffraction of a monocrystal. The IR spectrum shows a wide band at 2943 cm^{-1}

corresponding to Csp^2–H and Csp^3–H stretching bands. Alkene C–C stretching appears at 1584 cm^{-1}. A strong band at 1060 cm^{-1} corresponds to the B–F stretching of the BF_4 anion.

The $^{31}P\{1H\}$ NMR spectrum (Figure 11) shows two doublets of doublets at +2.9 and −42.6 ppm corresponding to P^2 and P^1, respectively, (P^1: $J_{P\text{-}Rh}$ = 142.8 Hz, P^2: $J_{P\text{-}Rh}$ = 131.9 Hz; $J_{P1\text{-}P2}$ = 63.4 Hz). The peaks are doublets of doublets because of the coupling between the two phosphorus and between phosphorus and rhodium. The absence of more peaks indicates that bischelated complexes (Figure 10) were not formed.

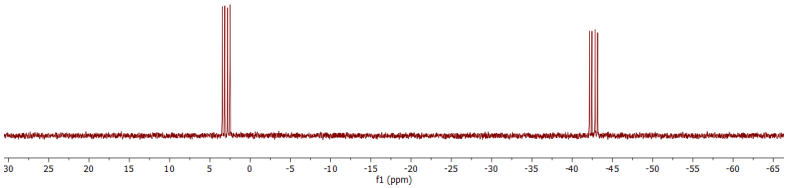

Figure 11. $^{31}P\{^1H\}$ NMR spectrum (162 MHz, CD_2Cl_2) of $\mathbf{C_1^1}$.

The ^1H NMR spectrum shows various signals from 7.7 to 6.8 ppm corresponding to the aromatic protons. Methylene bridge appears as two differentiated multiplets at 1.72 and 1.67 ppm. Norbornadiene shows four broad multiplets between 5.9 and 5.4 ppm corresponding to alkene hydrogens, Csp^3–H protons appear as two multiplets at 4.1 and 4.2 ppm and the CH_2 appear as two multiplets at 3.8 and 3.6 ppm.

Monocrystals of $\mathbf{C_1^1}$ were grown by diffusion of hexane in a solution of the complex in DCM. The crystals were analysed by XRD, which confirmed the expected structure of $\mathbf{C_1^1}$ (Figure 12).

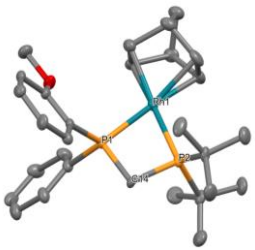

Figure 12. Plot of $\mathbf{C_1^1}$ with ellipsoids drawn at 50 % probability. H atoms and the BF_4 anion have been removed for clarity.

	Distance [Å]
P1-Rh1	2.3031(16)
P2-Rh1	2.3403(18)
P1-C14	1.847(6)

	Angle [°]
P1-Rh1-P2	72.37(6)
P1-C14-P2	96.00(3)

P2-C14	1.843(6)

Table 1. Most significant parameters of the $\mathbf{C_1^1}$ crystal structure.

The structure is composed of discrete units of the complex, in which the organometallic cationic has the anticipated square-planar geometry. The stereogenic phosphorus would have *S* absolute configuration in the free ligand, as expected.[19] The bite angle P^1–Rh–P^2 is 72.37°, which is in line with other methylene-bridged diphosphane-Rh(I) complexes.[9] The distance between the *P*-stereogenic atom and the rhodium atom is shorter than between P^2 and the rhodium because of the steric hindrance provided by the ^{t}Bu substituents.[19,27]

5.3. SYNTHESIS AND CHARACTERIZATION OF $\mathbf{C_3^1}$, $\mathbf{C_4^1}$ and $\mathbf{C_5^1}$

The last step of the catalyst synthesis was the pressurization of a solution of $\mathbf{C_1^1}$ in fluorobenzene under 4 bar of H_2, in order to hydrogenate the norbornadiene double bonds. Then, fluorobenzene should occupy the vacancy, to give $\mathbf{C_3^1}$. However, the characterization of the obtained solid, especially the $^{31}P\{^1H\}$ NMR spectrum, indicated that a mixture of compounds was obtained, in which the desired complex $\mathbf{C_3^1}$ was present (Scheme 10).

To study if the diene ligand influenced the reaction, complex $\mathbf{C_2^1}$ with cod was synthesised from $[Rh(cod)_2]BF_4$, following the same methodology for the synthesis of $\mathbf{C_1^1}$. The corresponding hydrogenation of $\mathbf{C_2^1}$ was performed under the same conditions but, unfortunately, a similar mixture of products was obtained (Scheme 10). From an $\mathbf{C_2^1}$ NMR tube that was left unattended a few days, yellow crystals were obtained. Their analysis by XRD, showed that they were a different structure, which resulted to be $\mathbf{C_1^0}$, a bis(PAMP) complex that has not been reported, so it was decided to synthesise this complex on purpose (see section 6.1).

From the mixture containing $\mathbf{C_3^1}$, a single crystal was obtained, which resulted to be a dimeric complex ($\mathbf{C_4^1}$) in which the phenyl groups of $\mathbf{L1}$ coordinate another rhodium moiety, stablishing an arene-rhodium bridge, acting as the ancillary ligand (Scheme 10 and Figure 13). Other similar dimeric structures have been described in the literature. For example, Bosnich and coworkers reported the complex $[Rh(dppe)]_2(ClO_4)_2$ where a phenyl from each dppe ligand coordinates another rhodium moiety.[14,28] Even more interesting is the dimer $[Rh(DIPAMP)]_2(BF_4)_2$; in this case, two different dimeric structures have been reported, a symmetric species where phenyl groups establish the arene-rhodium bridge, analogously to $\mathbf{C_4^1}$, and an unsymmetrical species in which one phenyl and one *o*-anisyl form the arene bridge.[24] There are no reported structures, however,

with single-atom bridged diphosphanes and hence $\mathbf{C_4^1}$ constitutes the first example. Interestingly, η^6-coordination with the rhodium takes place through the unsubstituted phenyl ring of $\mathbf{L1}$, despite the *o*-anisyl substituent being more electron-rich.

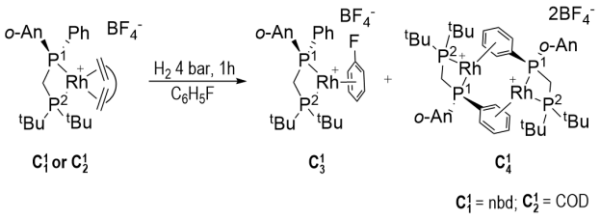

Scheme 10. Hydrogenation of $\mathbf{C_1^1}$ and $\mathbf{C_2^1}$.

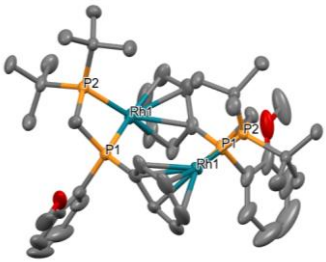

Figure 13. Plot of $\mathbf{C_4^1}$ with ellipsoids drawn at 50 % probability. H atoms and BF_4 anions have been removed for clarity.

The formation of $\mathbf{C_4^1}$ indicates that fluorobenzene is an excessively labile ligand to stabilize sufficiently $\mathbf{C_3^1}$. To achieve a pure catalytic precursor, another less labile ancillary ligand should be used. Consequently, fluorobenzene was substituted by acetonitrile, because in terms of lability acetonitrile falls between norbornadiene and fluorobenzene. The analogous **AmpaPhos**' catalyst, [Rh(**AmpaPhos**)$(NCMe)_2$]BARF has been tested by Willis, Weller, and coworkers, that results in slower reaction rate, although, high conversions were still achieved.[13]

5.3.1. Synthesis of $\mathbf{C_5^1}$

$\mathbf{C_1^1}$ was dissolved in fluorobenzene inside a Fisher-Porter tube and the solution was pressurized under 4 bar of H_2 for 1 h. To recrystallize the product, pentane was added to the solution to induce the product precipitation. The supernatant solvents were removed by decantation. The expected mixture of $\mathbf{C_3^1}$ and $\mathbf{C_4^1}$ was obtained, the solid was dissolved in MeCN and stirred for 5 minutes. The solvent was removed under vacuum (Scheme 11).

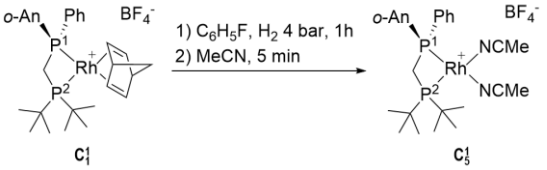

Scheme 11. Synthesis of $\mathbf{C_5^1}$.

5.3.2. Characterization of $\mathbf{C_3^1}$, $\mathbf{C_4^1}$ and $\mathbf{C_5^1}$

The mixture of $\mathbf{C_3^1}$ and $\mathbf{C_4^1}$ was characterized by ^{1}H, ^{31}P{^{1}H}, ^{13}C{^{1}H} NMR spectroscopy and COSY ^{1}H–^{1}H and HSQC H^{1}–^{13}C 2D NMR spectroscopy.

The ^{31}P{^{1}H} NMR spectrum of the mixture of $\mathbf{C_3^1}$ and $\mathbf{C_4^1}$ (Figure 14) shows two doublets of doublets at +22.0 and −26.2 ppm that can be assigned to complex $\mathbf{C_3^1}$. In addition, it contains a doublet of doublets centered at +15.4 ppm and a doublet of triplets at −17.3 ppm, corresponding to $\mathbf{C_4^1}$. Also, the presence of some initial $\mathbf{C_1^1}$ appears as two smaller doublets of doublets but optimizing the reaction parameters the presence of starting material could be avoided. The ^{31}P{^{1}H} NMR spectrum of $\mathbf{C_5^1}$ shows two doublets of doublets at +14.1 and −28.6 ppm, hence, the addition of acetonitrile affords a pure catalytic precursor.

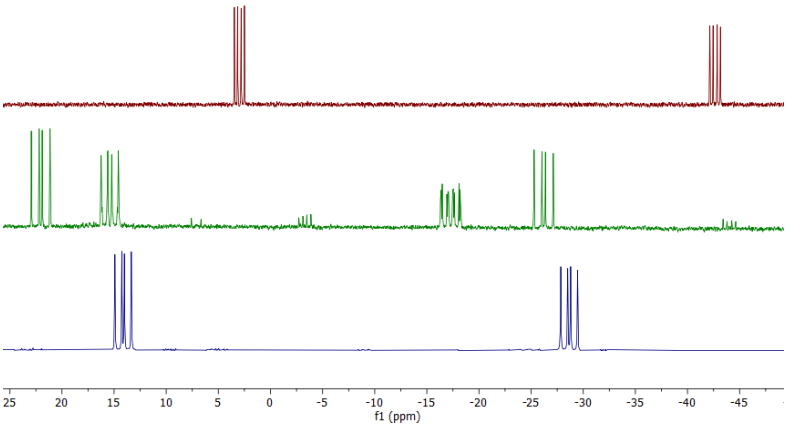

Figure 14. ^{31}P{^{1}H} NMR spectra (162 MHz) of $\mathbf{C_1^1}$ (CD_2Cl_2, top), of the mixture $\mathbf{C_3^1}$ + $\mathbf{C_4^1}$ (CD_3COCD_3, middle) and of $\mathbf{C_5^1}$ (CD_2Cl_2, bottom).

Analyzing the ^{1}H NMR spectrum of the $\mathbf{C_3^1}$ and $\mathbf{C_4^1}$ mixture, the duplicated peaks evidence the presence of two species: for example, two singlets at 3.6 and 3.5 ppm are assignable to two different methoxy groups and two multiplets at 2.5 and 1.7 ppm indicate two different methylene

bridge protons. Also, four doublets between 1.5 and 0.8 ppm show the presence of four different tert-butyl moieties. The ^{1}H NMR spectrum of $\mathbf{C_5^1}$ shows a singlet at 3.7 ppm that corresponds to methoxy protons. The bridge hydrogens appear as a multiplet at 3.3 ppm. Two broad peaks at 2.2 and 1.9 ppm corresponds to the six acetonitrile protons.

6. SYNTHESIS AND CHARACTERIZATION OF $\mathbf{C_1^0}$

The Rh(I) complex with **PAMP** (**L0**), denoted $\mathbf{C_1^0}$, is a bis(phosphane) complex that has not been previously reported, despite that PAMP was described in the late 1960s.[29] For this reason $\mathbf{C_1^0}$ was purposely prepared and characterized.

6.1. SYNTHESIS OF $\mathbf{C_1^0}$

A DCM solution of slightly more than 2 equivalents of $\mathbf{L0}$ was added dropwise to a DCM solution of $[Rh(cod)_2]BF_4$, and the yellow mixture was stirred for 2 h (Scheme 12), the solvent was removed by vacuum and the solid was recrystallized in DCM/Et_2O, to obtain the pure product. The final yield of $\mathbf{C_1^0}$ was 38 %.

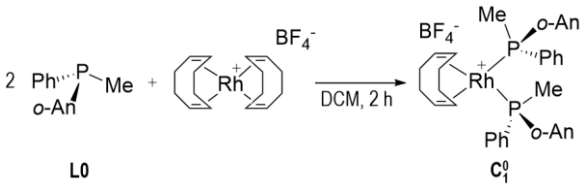

Scheme 12. Synthesis of $\mathbf{C_1^0}$.

6.2. CHARACTERIZATION OF $\mathbf{C_1^0}$

$\mathbf{C_1^0}$ was characterized by IR spectroscopy, ^{1}H, ^{31}P{^{1}H}, ^{13}C{^{1}H} NMR spectroscopy and COSY ^{1}H–^{1}H and HSQC H^1–^{13}C 2D NMR spectroscopy. The IR spectrum shows a peak at 3064 cm^{-1} corresponding to Csp^2–H stretching. Csp^3–H stretching appears as various peaks between 2965 and 2883 cm^{-1}. C–C alkene stretching band appears at 1585 cm^{-1}.

The $^{31}P\{^{1}H\}$ NMR spectrum shows a doublet at +9.4 ppm that corresponds to the equivalent phosphorus atoms coupled with rhodium ($J_{P\text{-}Rh}$ = 146.3 Hz). The absence of more peaks indicates the absence of other complexes. The ^{1}H NMR spectrum shows the aromatic protons as six signals between 8.0 and 6.5 ppm. A singlet at 3.9 ppm corresponds to the methoxy protons and a multiplet at 1.5 ppm are the two methyl hydrogen atoms.

Monocrystals of $\mathbf{C_1^0}$ were obtained from an NMR tube used to characterize $\mathbf{C_2^1}$, where $\mathbf{C_1^0}$ was found as an impurity (Figure 15).

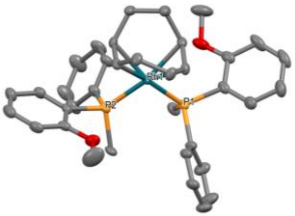

Figure 15. Plot of $\mathbf{C_1^0}$ with ellipsoids drawn at 50 % probability. H atoms and the BF_4 anion have been removed for clarity.

Parameter	Value
P1-Rh1	2.3157(16) Å
P2-Rh1	2.3194(16) Å
P1-Rh1-P2	90.67(6)º

Table 2. Most significant parameters of $\mathbf{C_1^0}$.

The angle P–Rh–P is 90.67º, the expected for a square planar structure. The distances between rhodium and phosphorus atoms are, also, the expected for a P–Rh bond.[14,19,27]

7. FLUORENE-BASED DIPHOSPHANES

The relative acidity of the hydrogen atoms of the fluorene CH_2 bridge allows to perform a deprotonation using a strong base, and by addition of the chlorophosphane a fluorene-monophosphane is obtained. Repeating the process fluorene-based diphosphane was produced in a one-pot synthesis (Scheme 13).

The studies of fluorene ligands started with the synthesis of the diphosphane **L2**, adapting the reported procedure of the literature.[23] Then, **L2** was complexed using $[Rh(cod)_2]BF_4$ to prepare $\mathbf{C_1^2}$ (**i**), which was obtained but not in a pure form. Literature results with the methylene-bridged ligand **dcpm** ($(Cy_2P)CH_2(PCy_2)$) indicates that the **L2** catalyst with fluorobenzene as ancillary ligand ($\mathbf{C_2^2}$) should be formed,[16] but the hydrogenation of (impure) $\mathbf{C_1^2}$ results in the decomposition of the product (**ii**). Finally, a direct reaction of a solution of **L2**, $[Rh(cod)_2]$BARF under hydrogen atmosphere in fluorobenzene to give $\mathbf{C_3^2}$ was also attempted, giving an unknown complex ($\mathbf{C_4^2}$) that is still under study (**iii**) (Scheme 13).

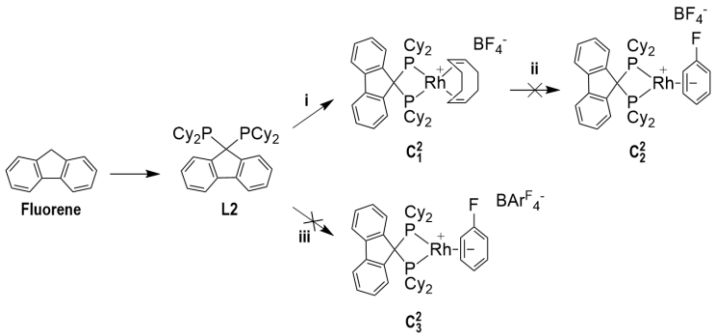

Scheme 13. Fluorene-based diphosphane **L2** and its complexes.

7.1. SYNTHESIS AND CHARACTERIZATION OF L2

L2 is a symmetric diphosphane that has been previously reported,[23] but its full characterization has not. To study the effect of the rigid fluorene backbone in catalysis, **L2** is an interesting ligand, since the analogous methylene-bridge diphosphane, **dcpm**, has been typically used intermolecular hydroacylation reactions reaching excellent results.[16]

7.1.1. Synthesis of L2

The preparation of **L2** was carried out by a modified literature procedure (Scheme 14).[23] Fluorene was dissolved in Et_2O, and using *n*-BuLi fluorene CH_2 was monodeprotonated. PCy_2Cl was added, the mixture was stirred overnight, and the solvent was removed under vacuum to furnish the monophosphane, which was not isolated. The monophosphane was redissolved in THF and fluorene was deprotonated again using *n*-BuLi and PCy_2Cl was added to obtain the diphosphane **L2**. The combined yield was 60 %.

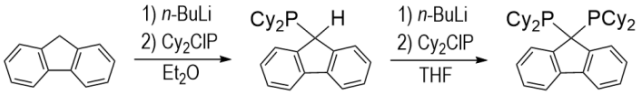

Scheme 14. Synthesis of **L2**.

7.1.2. Characterization of L2

L2 has been characterized by ^{1}H, $^{31}P\{^{1}H\}$ and $^{13}C\{^{1}H\}$ NMR spectroscopy, COSY ^{1}H–^{1}H and HSQC H^{1}–^{13}C 2D NMR spectroscopy and by HRMS.

The $^{31}P\{^{1}H\}$ NMR spectrum (Figure 16) shows two doublets at +23.5 and −2.4 ppm, the latter considerably broader than the former, corresponding to the two phosphorus atoms. Both phosphorus should be chemically equivalent, however, due to the rigidity of the fluorene backbone, they are not and, consequently, appear coupled. The coupling constant is abnormally large ($J^{2}_{P\text{-}P}$ = 308.8 Hz), which can be explained by a through-space coupling. TS spin couplings are couplings between two nonbonded atoms with overlapped lone pairs. This can occur when the structure is very rigid (Figure 17).[22]

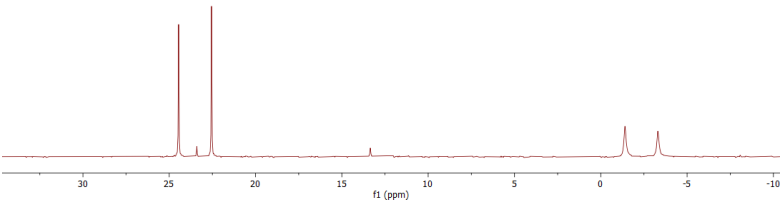

Figure 16. $^{31}P\{^{1}H\}$ NMR spectrum (162 MHz, CD_2Cl_2) of **L2**.

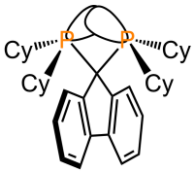

Figure 17. **L2** structure for a through-space coupling.

Increasing the temperature a $^{31}P\{^{1}H\}$ NMR experiment was performed to see whether coalescence was observed, but no significant changes were seen. In the reported synthesis of **L2** they interpret the $^{31}P\{^{1}H\}$ NMR (202 MHz, $CDCl_3$) as two singlets at 26.6 and 25.0 ppm, the observed doublet at a higher field was not reported, although they can be seen in the supporting information.[23] This is consequent to the spectrum reported in this TFG if the two reported singlets are considered as a doublet.

7.2. SYNTHESIS AND CHARACTERIZATION OF $\mathbf{C_1^2}$

7.2.1. Synthesis of $\mathbf{C_1^2}$

To a solution of $[Rh(cod)_2]BF_4$ in dichloromethane, a solution of $\mathbf{L2}$ was added dropwise. The mixture was stirred for 1 h. The obtained orange suspension was filtered through Celite, and the solvent was removed by vacuum. Purification was attempted by recrystallization in DCM/Et_2O and in DCM/hexane, however, due to the high solubility of the complex in DCM there was no precipitation of the product. A pure complex could not be obtained (Scheme 15).

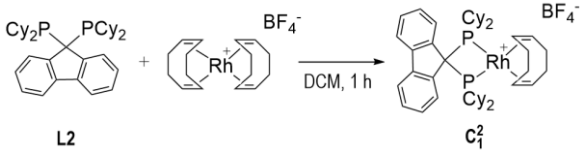

L2 $\mathbf{C_1^2}$

Scheme 15. Synthesis of $\mathbf{C_1^2}$.

7.2.2. Characterization of $\mathbf{C_1^2}$

$\mathbf{C_1^2}$ was characterized by $^{31}P\{^1H\}$ and ^1H NMR spectroscopy. The $^{31}P\{^1H\}$ NMR spectrum shows the complex as a doublet ($J_{Rh\text{-}P}$ = 144.1 Hz) at +38.2 ppm, a doublet at +164.7 ppm (J = 175.3 Hz) indicate the presence of an unknown product. The reported characterization of the analogous $[Rh(\mathbf{L2})(nbd)]BF_4$ complex shows a doublet at 17.0 ppm with a coupling constant $J_{Rh\text{-}P}$ = 135 Hz.[23]

The ^1H-NMR shows the fluorene aromatic protons as two multiplets between 7.9 and 7.3 ppm. Alkene cod hydrogens appear as a doublet and a singlet at 5.8 and 5.4 ppm, respectively. Cyclohexyl and alkane cod protons appear overlapped as a broad peak between 2.6 and 0.7 ppm.

7.3. SYNTHESIS AND CHARACTERIZATION OF $\mathbf{C_4^2}$

The hydrogenation of $\mathbf{C_1^2}$ did not enable the synthesis of $\mathbf{C_2^2}$, probably because the starting complex was not obtained pure. The $^{31}P\{^1H\}$ NMR spectrum of the obtained product shows various non-assignable signals between +58 and +33 ppm. Then a different method was studied to prepare the $\mathbf{C_3^2}$ complex, by hydrogenating a solution of $\mathbf{L2}$ and the rhodium precursor in fluorobenzene.

7.3.1. Synthesis of $\mathbf{C_4^2}$

Inside a Fischer-Porter **L2** and the rhodium precursor, [Rh(cod)$_2$]BARF, were dissolved in fluorobenzene. The solution was pressurized under 4 bar of H_2 for 20 minutes. The product was recrystallized by the addition of hexane. After two days a brown solid had precipitated.

7.3.2. Characterization of $\mathbf{C_4^2}$

The product was characterized by $^{31}P\{^1H\}$, ^1H, $^{13}C\{^1H\}$ and $^{19}F\{^1H\}$ NMR spectroscopy and by COSY ^1H–^1H, NOESY ^1H–^1H and HSQC H^1–^{13}C 2D NMR spectroscopy. The studies determined that the expected complex $\mathbf{C_3^2}$ was not formed.

The $^{31}P\{^1H\}$ NMR spectrum (Figure 18) shows a major species as two doublets of doublets at +88.5 (J = 178.7, 18.5 Hz) and −31.8 ppm (J = 178.6, 136.9 Hz) and a minor species as two doublets of doublets at +95.7 (J = 173.3, 29.8 Hz) and −17.9 ppm (J = 197.6, 173.5 Hz). Regarding the major species, although both P atoms should be equivalent, there are not, as occurs with **L2**. The larger coupling should be coupling constant between the two phosphorus nuclei and the smaller coupling constant should be P–Rh coupling constant. The peak at lower field is at unusual chemical shift and the anticipated P–Rh coupling constant is smaller than the reported for diphosphane ligands. Usually, P–Rh coupling constant are near 130 Hz, this indicates that probably one phosphorous is not directly bonded to the rhodium center. In the fluorine NMR, the BARF is clearly seen (δ_F = −62.86 ppm) a very small peak attributable to fluorobenzene (δ_F = −113.90 ppm) is observed, pointing that the substitution of COD has not taken place. It seems clear that the spectrum cannot correspond to the expected complex $\mathbf{C_3^2}$ and therefore it belongs to an unknown species, labelled as $\mathbf{C_4^2}$.

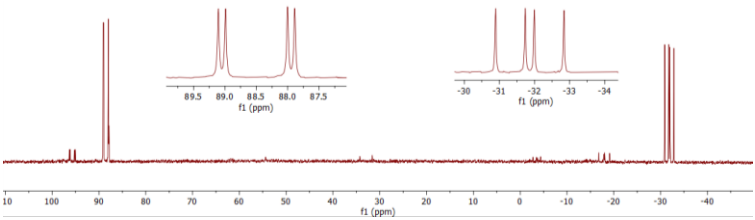

Figure 18. $^{31}P\{^1H\}$ NMR (162 MHz, CD_2Cl_2) of complex $\mathbf{C_4^2}$.

The most interesting signal in ^1H NMR is a singlet, that integrates 2 H, at 4.5 ppm, which indicates the presence of a non-aromatic double C–C bond. This peak could correspond to a cod that only one C=C has been hydrogenated or to a COD ligand.

A possible explanation for the differentiation of P atoms is the monooxidation of the ligand, leading to a Rh-O coordination, that would also explain the small P-Rh coupling constant (Figure 19, left). Nevertheless, this option is unlikely because typically the $J_{P\text{-}P=O}$ that have been described are near to 50 Hz.[25]

Another hypothesis is that the double bond has been formed by a spontaneous intermolecular dehydrogenation of a cyclohexyl group of the phosphane (Figure 19, right). Dehydrogenation is a reaction that permits to activate alkanes to continue with their functionalization and provide synthetically useful products. Homogeneous dehydrogenation process can be performed using transition metal complexes[30,31] (Scheme 16). The dehydrogenation of $\mathbf{C_3^2}$ cyclohexyl would lead to a *P*[1]-stereogenic complex $\mathbf{C_4^2}$, where a P substituent is a cyclohexenyl rhodium coordinating with an η^2 hapticity (Figure 19, right).

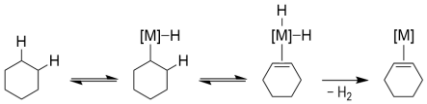

Scheme 16. Dehydrogenation reaction.

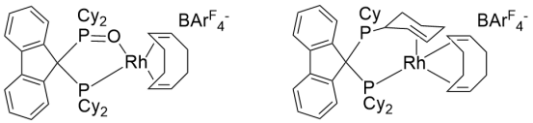

Figure 19. Possible structures of $\mathbf{C_4^2}$.

The identity of $\mathbf{C_4^2}$ remains speculative, but a brown crystal has been grown and submitted for X-ray diffraction analysis, with the hope that it could shed light into the nature of this complex.

8. CATALYSIS

8.1. ENANTIOSELECTIVE HYDROGENATION

Following previous studies on enantioselective hydrogenation,[19] $\mathbf{C_1^1}$ and $\mathbf{C_1^0}$ were tested as catalytic precursors with three typical substrates methyl (*Z*)-α-acetamidocinnamate (*Z*-MAC) (**S1**), ethyl α-acetamidoacrylate (MAA) (**S2**), and dimethyl itaconate (DMI) (**S3**).

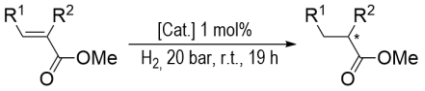

S1: R^1 = Ph, R^2 = NHAc ((*Z*)-MAC); **S2**: R^1 = H, R^2 = NHAc (MAA); **S3**: R^1 = H, R^2 = CH_2CO_2Me (DMI)

Entry	Catalyst	Substrate	Conv. [%]	ee [%]
1	$\mathbf{C_1^0}$	S1	>99	44 (*R*)
2		S2	>99	36 (*R*)
3		S3	98	27 (*S*)
4	$\mathbf{C_1^1}$	S1	>99	16 (*R*)
5		S2	>99	55 (*R*)
6		S3	>99	58 (*S*)

Reaction conditions: 0.2 M substrate, THF, 1 mol% catalyst, 20 bar H_2, rt, 19 h.

Table 3. Results of enantioselective hydrogenation.

As can be seen in Table 3, both catalysts achieve full conversions for all substrates. The catalysis with $\mathbf{C_1^0}$ achieved low enantiomeric excess for the three alkenes. $\mathbf{C_1^1}$ achieve better results for MAA and DMI but reaching only a modest enantiomeric excess. On the other hand, Z-MAC did not follow the trend, better results were achieved with the bisphosphane catalyst $\mathbf{C_1^0}$.

Knowles and coworkers used, in enantioselective hydrogenation, the complex [Rh(**L0**)(cod)(Cl)]BF_4 adding an equivalent of **L0** *in situ*. Reported enantiomeric excess, for different functionalized olefins, range between 50 and 60 %, but has not been tested for the three substrates explored here.[7,8]

8.2. INTERMOLECULAR HYDROACYLATION

Rhodium complex $\mathbf{C_5^1}$ was tested in intermolecular hydroacylation. The chosen substrates were 1-octene (**S4**) and 1-octyne (**S5**), that are typically used in catalysis, and as internal alkenes two cyclic enol ethers were chosen, 2,3-dihydrofuran (**S6**) and 3,4-dihydro-2H-pyran (**S7**) (Figure 20). β-(methylthio)benzaldehyde (**1**) has been used in all the reactions as the aldehyde.

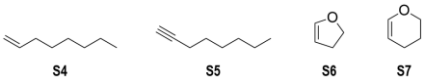

Figure 20. Hydroacylation substrates.

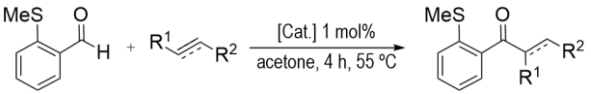

Entry	Substrate	Product	Ligand	Loading [mol%]	Conv. [%]	Select. [%]
1	S4	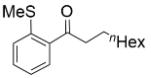	**L1**	1	99	75
			Ampaphos[a]	1.3	>95	>99
2	S4	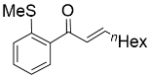	**L1**	1	93	>99
3	S6	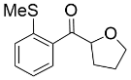	**L1**	1	>99	>99
			Ampaphos[b]	1	94	>99
4	S7	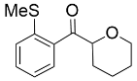	**L1**	1	32	>99
			Ampaphos[b]	3	94	>99

Reaction conditions: aldehyde (2.0 M, 1 eq.), substrate (1.5 eq.), acetone (0.15 mL), 1 mol% catalyst, 55 ºC, 4 h. [a]: aldehyde (1.5 M, 1 eq.), substrate (2.7 eq.), acetone, 0.02 M catalyst, 25 ºC, 5 min. [b]: aldehyde (2.0 M, 1 eq.), substrate (1.5 eq.), acetone, 55 ºC, 3 h.

Table 4. Catalytic hydroacylation results with **L1** and **Ampaphos**.[13]

The results shown in Table 4, indicate that for the terminal unsaturated substrates, **S4** achieves a lower selectivity (3:1, linear:branched) than **S5** because in the latter substrate only the linear product was observed. On the other hand, **S4** reaches a better conversion than **S5**. Focusing on the internal alkenes, in both cases remarkable regioselectivity was achieved, in terms of conversion, **S6** reaches a high conversion, better than **S7**.

Comparing the results with Willis and Weller's catalyst [Rh(**AmpaPhos**)(C_6H_5F)]BARF, for **S4** a similar conversion was obtained using **L1**, in terms of regioselectivity, employing **AmpaPhos** only the linear product was observed, while using **L1** both linear and branched products were obtained. Hence, in this case **L1** achieved a lower selectivity. Focusing on the cyclic enol ethers, **Ampaphos** also achieve an exceptional regioselectivity. **L1** has reached better conversion results for **S6** at the same experimental conditions, however, **S7** conversion was notably lower using **L1** than the achieved results with **AmpaPhos**. However, the results cannot be directly compared, since, in this case Willis and Weller used a higher catalyst loading, which indicates that **S7** is a more challenging substrate than **S6**.[13] These preliminary results demonstrate that **L1** furnishes similar results than **Ampaphos** in terms of activity and regioselectivity. However, **L1** is a chiral, optically pure ligand and therefore could produce enantioenriched products. The separation and quantification of the hydroacylation with substrates **S6** and **S7** to evaluate the enantioselectivity are in course in the research group.

9. STERIC PROPERTIES OF L1

The steric properties of the ligands are evaluated using various parameters as the Tolman cone angle (Figure 21), the percent of the buried volume (*%V*$_{bur}$) or the steric map.[32] The Tolman cone angle is defined as the cone angle formed with the metal center at the vertex and the edges extending to the Van der Walls spheres of the outermost atoms. The *%V*$_{bur}$ is the occupied volume for a given ligand of a sphere centered on the metal. The steric map is the representation of *%V*$_{bur}$ along the xy surface.[32]

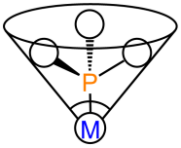

Figure 21. Tolman cone angle. The P–M distance is arbitrarily fixed at 2.28 Å.

To study the steric properties of **L1**, *%V*$_{bur}$ and the topographic steric map were calculated (Figure 22). It is reasonable to assume that high differentiation in quadrants *%V*$_{bur}$, is related to high enantioselectivities in hydrogenation. The *%V*$_{bur}$ of 49.7 indicates that **L1** is a bulky ligand, and, also, that the difference between the *P*-stereogenic quadrants (NE and SE) is moderate.

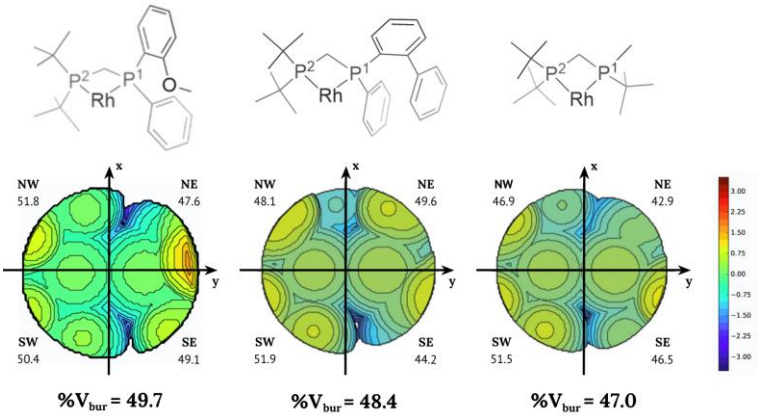

Figure 22. Steric maps of **L1** (left), **L3** (center), **TCFP** (right).

The results have been compared, with ligand **L3**, previously synthesised by the group, and, also, with the **TCFP**, which is a highly enantioselective diphosphane ligand for hydrogenation[19,26] (Figure 22). The values of *%V*$_{bur}$ indicate that **L1** is a bulkier ligand than **L3** and **TCFP**. Calculating the ratio between quadrants, [*%V*$_{bur}$(NW) + *%V*$_{bur}$(SW)] : [*%V*$_{bur}$(NE) + *%V*$_{bur}$(SE)], are 100:95, 100:94 and 100:91 for **L1**, **L3** and **TCFP** respectively. The ratio shows that the difference

between W and E halves is slightly smaller for **L1**. The results suggest that the low %*ee* achieved in catalysis could be explained because the buried volume difference quadrants of **L1** is not large enough.

10. EXPERIMENTAL SECTION

10.1. MATERIALS AND METHODS

All compounds were synthesised under a purified nitrogen atmosphere employing standard Schlenk and vacuum line techniques or inside the glovebox. The used solvents were acquired from a solvent purificator. NMR spectra, including ^{1}H, ^{13}C{^{1}H}, ^{19}F{^{1}H}, ^{31}P{^{1}H}, and bidimensional were recorded using a 400 MHz spectrometer and the fields are 400 MHz 1H, 101 MHz ^{13}C{^{1}H}, 376 MHz ^{19}F, and 162 MHz ^{31}P{^{1}H} with the specified purified solvent. IR spectra were recorded with an ATR. HRMS analyses were performed using electrospray ionization. The catalytic runs were chromatographically analysed using GC. Steric properties have been calculated using SambVca 2.1 web application.

10.2. L1: PREPARATION OF THE LIGAND AND ITS COMPLEXES

10.2.1. Synthesis of L1

L0 · BH$_3$ (122 mg, 0.5 mmol) was dissolved in 5 mL of THF and the solution was cooled to −30 ºC. *S*-BuLi (1.6 M solution, 0.5 mL, 0.75 mmol, 1,3 eq.) was added, and the mixture was stirred for 1 h. Then, ^{t}Bu$_2$PCl (0.15 mL, 0.65 mmol, 1 eq.) was added and the reaction was stirred for 1 h. The solution was taken out of the cold bath and was stirred for 30 min. After, ^{i}PrOH was added to quench the unreacted *sec*-BuLi and the solution was brought to dryness. The product was dissolved in morpholine and stirred for 24 h. Solvent was evaporated, the remaining solid was dissolved in toluene (4 x 2.5 mL) and eluted through alumina to separate the product from the morpholine-borane adduct. Toluene was removed under vacuum yielding **L1** as pasty solid.

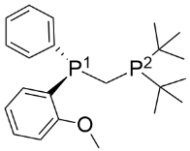

^{1}H NMR ($CDCl_3$, 400 MHz). δ 7.59-7.52 (m, 2H, Ar), 7.35-7.28 (m, 4H, Ar), 7.23-7.16 (m, 1H, Ar), 6.93 (t, *J* = 7.5 Hz, 1H, Ar), 6.84 (dd, *J* = 8.3, 3.8 Hz, 1H, Ar), 3.75 (s, 3H, CH_3O), 2.31 (ddd, *J* = 13.9, 4.6, 1.6 Hz, 1H, $CH_{2(bridge)}$), 1.98 (d, *J* = 14.0 Hz, 1H, $CH_{2(bridge)}$), 1.23 (d, *J* = 11.0 Hz, 9H, $CH_{3(tBu)}$), 1.02 (d, *J* = 11.0 Hz, 9H, $CH_{3(tBu)}$). **^{13}C{^{1}H} NMR ($CDCl_3$, 101 MHz).** δ 159.91-119.8 (m, 12C, Ar), 54.36 (s, 1C, CH_3O), 31.08 (dd, *J* = 23.3, 4.6 Hz, 2C, C_{tBu}), 28.84 (dd, *J* = 13.2, 3.6 Hz, 3C, $CH_{3(tBu)}$), 28.54 (d, *J* = 13.5 Hz, 3C, $CH_{3(tBu)}$), 17.34 (dd, *J* = 32.4, 20.4 Hz, 1C, $CH_{2(bridge)}$). **^{31}P{^{1}H} NMR ($CDCl_3$, 162 MHz).** δ 17.46 (d, *J* = 141.9 Hz, P^2), −23.68 (d, *J* = 142.1 Hz, P^1).

10.2.2. Synthesis of $\mathbf{C_1^1}$

A solution of **L1** (187 mg, 0.5 mmol) in 5 mL of DCM was added dropwise over a solution of $[Rh(nbd)_2]BF_4$ (147 mg, 0.385 mmol, 0.77 eq.) in 5 mL of DCM for 20 min. The mixture was stirred for 1 h. The solution was brought to dryness and the product was recrystallized in DCM/Et_2O overnight in the freezer. The product was filtered and washed with cold pentane. Yield: 24 % (120 mg).

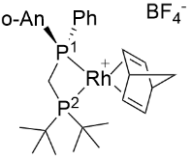

H NMR (CD_2Cl_2, 400 MHz). δ 7.67 (ddd, *J* = 13.2, 7.6, 1.7 Hz, 1H, Ar), 7.55-7.35 (m, 6H, Ar), 6.87 (ddd, *J* = 8.4, 4.5, 1.0 Hz, 1H, Ar), 5.94 (m, 1H, $CH_{(nbd)}$), 5.77 (m, 1H, $CH_{(nbd)}$), 5.45 (m, 1H, $CH_{(nbd)}$), 5.41 (m, 1H, $CH_{(nbd)}$), 4.21 (m, 1H, $CH_{(nbd)}$), 4.16 (m, 1H, $CH_{(nbd)}$), 3.83 (m, 1H, $CH_{2(nbd)}$), 3.55 (m, 1H, $CH_{2(nbd)}$), 3.50 (s, 3H, CH_3O), 1.71 (m, 1H, $CH_{2(bridge)}$), 1.67 (m, 1H, $CH_{2(bridge)}$), 1.24 (d, *J* = 2.6 Hz, 9H, $CH_{3(tBu)}$), 1.20 (d, *J* = 2.7 Hz, 9H, $CH_{3(tBu)}$). **^{13}C{^{1}H} NMR (CD_3Cl, 101 MHz).** δ 160.63 (s, 1C, Ar_{CO}), 134.22-112.16 (m, 11C, Ar), 92.31 (m, 1C, $CH_{(nbd)}$), 90.12 (m, 1C, $CH_{(nbd)}$), 87.89 (m, 1C, $CH_{(nbd)}$), 87.10 (m, 1C, $CH_{(nbd)}$), 70.61 (s, 1C, $CH_{2(bridge)}$), 56.39 (s, 1C, $CH_{(nbd)}$), 56.12 (s, 1C, $CH_{(nbd)}$), 55.91 (s, 1C, CH_3O), 33.49 (s, 1C, $CH_{2(nbd)}$), 30.59 (s, 2C, $C_{(tBu)}$), 29.34 (d, *J* = 5.8 Hz, 3C, CH_{3tBu}), 28.95 (d, *J* = 5.8 Hz, 3C, CH_{3tBu}). **^{31}P{^{1}H} NMR (CD_2Cl_2, 162 MHz).** δ 2.98 (dd, *J* = 131.9, 63.4 Hz, P_2), −42.65 (d, *J* = 142.8, 63.3 Hz, P_1). **IR.** 2943, 1459, 1434, 1160, 759, 710.

10.2.3. Synthesis of $\mathbf{C_2^1}$

$\mathbf{C_2^1}$ was prepared analogously to $\mathbf{C_1^1}$ with $[Rh(cod)_2]BF_4$ (154 mg, 0.28 mmol). Yield: 62 % (208 mg).

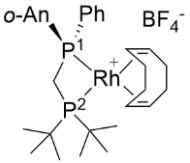

^{1}H NMR (CD_2Cl_2, 400 MHz). δ 7.75 (ddd, *J* = 13.1, 7.6, 1.7 Hz, 1H), 7.55 (m, 1H, Ar), 7.49-7.33 (m, 4H, Ar), 7.14 (tdd, *J* = 7.5, 1.9, 1.0 Hz, 1H, Ar), 6.92 (d, *J* = 8.3 Hz, 1H, Ar), 5.73 (m, 2H, $CH_{(cod)}$), 5.01 (m, 2H, $CH_{(cod)}$), 3.48 (s, 3H, CH_3O), 2.31 (m, 8H, $CH_{2(cod)}$), 1.68 (br, 2H, $CH_{2(bridge)}$), 1.28 (d, *J* = 12.3 Hz, 9H, $CH_{3(tBu)}$), 1.25 (d, *J* = 12.3 Hz, 9H, $CH_{3(tBu)}$). **^{13}C{^{1}H} NMR (CD_3Cl, 101 MHz).** δ 160.81 (s, 1C, Ar_{CO}), 134.84-112.39 (m, 11C, Ar), 101.15 (dd, *J* = 9.1, 6.8 Hz, $CH_{(cod)}$), 100.01 (dd, *J* = 10.0, 6.3 Hz, $CH_{(cod)}$), 97.76 (t, *J* = 8.1 Hz, $CH_{(cod)}$), 95.09 (dd, *J* = 9.4, 7.3 Hz, $CH_{(cod)}$), 68.80 (s, 1C, $C_{(bridge)}$), 55.80

(s, 1C, CH_3O), 36.74 (d, J = 8.2 Hz, 1C, $C_{(tBu)}$), 36.17 (m, 1C, $C_{(tBu)}$), 30.37 (d, *J* = 14.6 Hz, 2C, $CH_{2(cod)}$), 29.93 (d, *J* = 44.0 Hz, 2C, $CH_{2(cod)}$), 29.62 (d, *J* = 5.4 Hz, 5C, $CH_{3(tBu)}$), 29.26 (d, *J* = 5.1 Hz, 3C, $CH_{3(tBu)}$). **$^{31}P\{^1H\}$ NMR (CD_3Cl, 162 MHz).** −3.28 (dd, *J* = 125.0, 61.8 Hz, P^2), −43.35 (dd, *J* = 134.3, 61.6 Hz, P^1).

10.2.4. Synthesis of $\mathbf{C_5^1}$

$\mathbf{C_1^1}$ (64 mg, 0.17 mmol) was dissolved in 2 mL of fluorobenzene inside a Fisher-Porter tube The solution is stirred under 4 bar H_2 pressure. After 20 min, pentane was added to the solution, the solid was allowed to precipitate during 72 h. Then, the solvent was decanted and the solid was dried under vacuum, the mixture $\mathbf{C_3^1}$ + $\mathbf{C_4^1}$ was obtained. The solid was dissolved in 5 mL of acetonitrile and stirred for 5 min. The solution was brought to dryness.

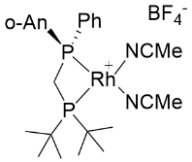

^1H NMR (CD_2Cl_2, 400 MHz). δ 8.21 (ddd, *J* = 16.0, 7.5, 1.8 Hz, 1H, Ar), 7.69 (m, 2H, Ar), 7.42 (m, 1H, Ar), 7.31 (m, 3H, Ar), 7.04 (tdd, *J* = 7.5, 1.9, 1.0 Hz, 1H, Ar), 6.78 (dd, *J* = 8.4, 3.5 Hz, 1H, Ar), 3.66 (s, 3H, CH_3O), 3.28 (m, 2H, $CH_{2(bridge)}$), 2.24 (br, 3H, $CH_{3(NCMe)}$), 1.89 (br, 3H, $CH_{3(NCMe)}$), 1.24 (d, *J* = 14.3 Hz, 9H, $CH_{3(tBu)}$), 1.14 (d, *J* = 14.3 Hz, 9H, $CH_{3(tBu)}$). **$^{13}C\{^1H\}$ NMR (CD_2Cl_2, 101 MHz.** δ 158.52 (s, 1C, Ar_{CO}), 137.84-107.08 (m, 11C, Ar), 115.86 (s, 2C, NC), 54.52 (s, 1C, CH_3O), 34.1 (t, *J* = 8.2 Hz, 1C, $C_{(tBu)}$), 33.12 (dd, *J* =27.7, 17.8 Hz, 1C, $C_{(tBu)}$), 28.19 (dd, *J* = 9.2, 5.1 Hz, 5C, $CH_{3(tBu)}$), 2.45 (d, *J* = 20.5 Hz, 1C, CH_3), 0.90 (s, 1C, CH_3). **$^{31}P\{^1H\}$ NMR (CD_2Cl_2, 162 MHz).** δ 14.13 (dd, J = 147.3, 107.6 Hz, P^2), −28.65 (dd, J = 153.7, 107.6 Hz, P^1).

10.3. Study of $\mathbf{C_1^0}$

$\mathbf{L0 \cdot BH_3}$ (63 mg, 0.25 mmol) was dissolved in 5 ml of morpholine and stirred overnight and the solvent was removed under vacuum. $\mathbf{L0}$ (PAMP) was dissolved in 10 mL of DCM and added dropwise to a solution of $[Rh(cod)_2]BF_4$ (31 mg, 0.075 mmol, 0.3 eq.) in 5 mL of DCM. After 2 h of stirring the solution was brought to dryness and the product was recrystallized in DCM/Et_2O. Yield: 38% (22 mg).

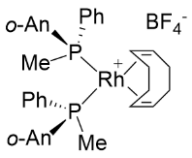

^1H NMR (CD_2Cl_2, 400 MHz). δ 7.94 (br, 4H, Ar), 7.62-7.52 (m, 4H, Ar), 7.38 (m, 2H, Ar), 6.94 (m, 2H, Ar), 6.81 (t, *J* = 7.4 Hz, 2H, Ar), 6.62 (q, *J* = 4.42 Hz, 2H, Ar), 4.50 (m, 2H, $CH_{(cod)}$), 4.20 (q, *J* = 7.4 Hz , 2H, $CH_{(cod)}$), 3.90 (s, 6H, CH_3O), 2.52-2.24 (m, 4H, $CH_{2(cod)}$), 2.14-2.03 (m, 4H, $CH_{2(cod)}$), 1.46 (m, 6H, CH_3). **$^{13}C\{^1H\}$ NMR (CD_2Cl_2, 101 MHz).** δ 159.94 (s, 2C, Ar_{CO}), 135.06-111.52 (m, 22C, C_{Ar}), 98.99 (m, 2C, $CH_{(cod)}$), 97.53 (m, 2C, $CH_{(cod)}$), 55.84 (s, 2C, C_{MeO}), 32.55 (s, 2C, $CH_{2(cod)}$), 29.08 (s, 2C, $CH_{2(cod)}$), 14.53-14.19 (t, *J* = 17.3Hz, 2C, C_{Me}). **$^{31}P\{^1H\}$ NMR (CD_2Cl_2, 162 MHz).** δ: 9.78-9.05 (d, *J* = 146. 3 Hz, 2P). **IR.** 3064, 2965, 2883, 1584, 1473, 1434, 1190, 759. **HRMS (ESI).** *m/z* calc. for $[M]^+$ 671.5689 $C_{36}H_{42}O_2P_2Rh^+$; found 671.1701.

10.4. STUDIES OF FLUORENE-BASED LIGAND

10.4.1. Synthesis of L2

Fluorene (175 mg, 1 mmol) was dissolved in 20 mL of Et_2O, the solution was cooled to 0 ºC. *n*-BuLi (0.7 mL, 1.6 M, 1.15 mmol, 1.15 eq.) was added, the mixture was stirred for 30 min, then $PClCy_2$ (0.26 mL, 1.15 mmol, 1.15 eq.) was added. The suspension was stirred overnight, then, it was brought to dryness and the remaining solid was washed with methanol (3 x 4 mL). The product was dissolved in 10 mL of THF. The solution was cooled to 0 ºC and *n*-BuLi (1.6 M, 0.67 mL, 1.1 mmol, 1.1 eq) was added. After 30 min of stirring, $PClCy_2$ (0.25 mL, 1.10 mmol, 1.10 eq) was added, and the mixture was stirred overnight. The suspension was dried under vacuum and the solid was washed with Et_2O (3 x 4 mL). Yield: 60% (334 mg).

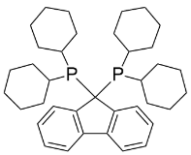

^{1}H NMR (C_6D_6, 400 MHz). δ 8.26 (d, *J* = 7.8 Hz, 2H, H_{Flu}), 7.62 (d, *J* = 8.3 Hz, 2H, H_{Flu}), 7.37 (ddd, *J* = 8.3, 6.9, 1.4 Hz, 2H, H_{Flu}), 7.14 (t, *J* = 6.9 Hz, 2H, H_{Flu}), 3.25 (q, *J* = 12.3 Hz, 2H, CH_{Cy}), 2.30-2.11 (m, 4H, $CH_{2(Cy)}$), 2.03-1.89 (m, 2H, $CH_{(Cy)}$), 1.87-0.60 (m, 36H, $CH_{2(Cy)}$). **^{13}C{^{1}H} NMR (C_6D_6, 101 MHz).** δ 140.45 (d, *J* = 13.3 Hz, 2C,C_{Flu}), 131.20 (d, *J* = 12.8 Hz, 2C, C_{Flu}), 122.50 (s, 2C, C_{Flu}), 119.32 (s, 2C, C_{Flu}), 116.10 (s, 2C, C_{Flu}), 115.39 (s, 2C, C_{Flu}), 54.21 (dd, J = 79.1, 3.2 Hz, 1C, C_{bridge}), 37.67 (dd, *J* = 39.8, 9.4 Hz, 2C, $CH_{(Cy)}$), 33.00 (dd, *J* = 20.6, 6.8 Hz, 2C, $CH_{(Cy)}$), 31.34 (dd, *J* = 23.2, 3.0 Hz, 2C, $CH_{2(Cy)}$), 30.12 (t, *J* = 6.5 Hz, 2C, $CH_{2(Cy)}$), 29.16 (dd, *J* = 12.4, 3.4 Hz, 2C, $CH_{2(Cy)}$), 28.67 (d, *J* = 4.3 Hz, 2C, $CH_{2(Cy)}$), 27.15 (t, *J* = 12.5 Hz, 4C, $CH_{2(Cy)}$), 26.87 (d, *J* = 13.7 Hz, 2C, $CH_{2(Cy)}$), 26.10 (d, *J* = 7.0 Hz, 2C, $CH_{2(Cy)}$), 25.30 (d, *J* = 27.4 Hz, 4C, $CH_{2(Cy)}$). **^{31}P{^{1}H} NMR (C_6D_6, 162 MHz).** δ 23.50 (d, *J* = 308.8 Hz, 1P), −2.36 (d, *J* = 308.9 Hz, 1P). **HRMS (ESI).** *m/z* calc. for $[M-H]^+$ 559.7622 $C_{37}H_{53}P_2^+$; found 559.3672.

10.4.2. Synthesis of C_1^2

L2 (59 mg, 0.1 mmol, 1 eq.) was dissolved in 5 mL of DCM and added dropwise to a solution of $[Rh(cod)_2]BF_4$ (44 mg, 0.1 mmol, 1 eq.). The solution was filtered through a dap of Celite and the solvent was removed under vacuum.

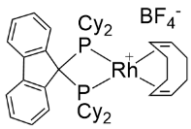

^{1}H NMR ($CDCl_3$, 400 MHz). δ 7.8 (m, 2H, Ar), 7.4 (m, 6H, Ar), 5.8 (d, *J* = 13.4 Hz, 2H, $CH_{(cod)}$), 5.6 (s, 2H, $CH_{(cod)}$), 2.65-0.40 (m, 52H, Cy + $CH_{2(cod)}$). **^{31}P{^{1}H} NMR ($CDCl_3$, 162 MHz).** δ 33.17 (d, *J* = 144.1 Hz, 2P).

10. CONCLUSIONS

P-stereogenic methylene-bridged diphosphane $\mathbf{L1}$ has been successfully synthesised from **PAMP·BH$_3$**. Its complexation studies with two Rh(I)-diene precursors have successfully furnished complexes $\mathbf{C_1^1}$ and $\mathbf{C_2^1}$, which have been fully characterized including the crystal structure of the former. In contrast, the hydrogenation of $\mathbf{C_1^1}$ and $\mathbf{C_2^1}$ complexes in fluorobenzene have not provided the expected complex $\mathbf{C_3^1}$ in a pure form, nevertheless, an interesting dimer ($\mathbf{C_4^1}$) has been obtained. This shows that fluorobenzene was probably not coordinating enough to stabilize sufficiently $\mathbf{C_3^1}$ to be isolated in a pure form. To circumvent this problem and obtain a pure catalytic precursor for hydroacylation, complex $\mathbf{C_5^1}$ was successfully prepared with acetonitrile as ancillary ligand. In addition, the unreported complex $\mathbf{C_1^0}$ with **PAMP** (**L0**) has been synthesized and fully characterized.

$\mathbf{C_1^1}$ and $\mathbf{C_1^0}$ have been tested as precursors in enantioselective hydrogenation with three benchmark substrates. In all cases, good activities but moderate enantiomeric excess were achieved. An explanation for the unselective nature of $\mathbf{C_1^1}$ has been provided by studying the steric properties of the ligand $\mathbf{L1}$.

$\mathbf{C_5^1}$ has been used in intermolecular hydroacylation of two terminal substrates, and two internal alkenes and the results are similar, in terms of activity and selectivity, to the ligand **AmpaPhos**. These satisfactory results, with the enantioselectivity still unknown, encourage further studies with prochiral substrates.

Fluorene-based diphosphane $\mathbf{L2}$ was synthesised. The NMR spectra indicates that phosphorus atoms were no equivalent and couple to each other, likely because of the high rigidity provided by the fluorene backbone. $\mathbf{L2}$ complexation with a Rh(I) precursor provides an impure $\mathbf{C_1^2}$ complex. Persisting on $\mathbf{L2}$ coordination a pressurization of a solution of the ligand and another Rh(I) was performed under H_2 atmosphere. The product obtained was not the expected $\mathbf{C_3^2}$, but an unknown species $\mathbf{C_4^2}$. It is possible that the ligand has suffered a dehydrogenation of a cyclohexyl group, leading to a *P*-stereogenic, diphosphane-diene ligand. The fluorene-based diphosphanes resulted to be more challenging than anticipated, and further studies are needed.

11. REFERENCES AND NOTES

1. Cornils, B.; Herrmann, W. A.; Beller, M.; Paciello, R. Applied Homogeneous Catalysis with Organometallic Compounds: A Comprehensive Handbook in Four Volumes. 3rd ed.; Wiley: New York, 2017; p 1872.
2. Van Leeuwen, P. Reference Module in Chemistry, Molecular Sciences and Chemical Engineering. Elsevier: Amsterdam, 2016; pp 1-45.
3. Osborn, J. A.; Jardine, F. H.; Young, J. F.; Wilkinson, G. J. The preparation and Properties of Tris(triphenylphosphino)halogenorhodium(I) and Some Reactions thereof including Catalytic Homogeneous Hydrogenation of Olefins and Acetylenes and their Derivatives. *J. Chem. Soc*. (A) **1966**, 1711-1732.
4. Vidal-Ferran, A.; Grabulosa, A.; Verdaguer, X.; Riera, A. Catalytic Asymmetric Synthesis. 4th ed.; Wiley: New York, 2022; pp 561-616.
5. Knowles, W. S. Asymmetric Hydrogenations (Nobel Lecture). *Angew. Chem. Int. Ed*. **2002**, 41, 1998-2007.
6. Noyori, R. Asymmetric Catalysis: Science and Opportunites (Nobel Lecture). *Angew. Chem. Int. Ed.* **2002**, 41, 2008-2022.
7. Knowles, W. S. Asymmetric Hydrogenation. *Acc. Chem. Res*. **1983**, 16, 106-112.
8. Knowles, W. S.; Sabacky, M. J.; Vineyard, B. D. Catalytic Asymmetric Hydrogenation. *J. Chem. Soc., Chem. Commun*. **1972**, 10-11.
9. Fernández, M.; Willis, M. C. Rhodium in Organic Synthesis: Methods and Reactions, 1st Ed.; Wiley: New York, 2019; pp 63-84.
10. Sakai, K.; Ide, J.; Oda, O.; Nakamura, N. Synthetic studies on prostanoids 1 synthesis of methyl 9-oxoprostanoate. *Tetrahedron Lett.* **1972**, 13, 1287-1290.
11. Lochow, C. F.; Miller, R.G. Transition-metal-promoted aldehyde-alkene addition reactions. *J. Am. Chem. Soc*. **1976**, 98, 1281-1283.
12. Willis, M. C. Comprehensive Organic Syntheis II, 2nd ed.; Elsevier: Amsterdam, 2014; Vol. 4; pp 961-994.
13. Prades, A.; Maitane, F.; Pike, S. D.; Willis, M. C.; Weller, A. S. Well-Defined and Robust Rhodium Catalysts for the Hydroacylation of Terminal and Internal Akenes. *Angew. Chem. Int. Ed.* **2015**, 127, 8520-8524.
14. Mansell, S. M. Catalytic applications of small bite-angle diphosphorus ligands with single-atom linkers. *Dalton Trans.* **2017**, 46, 15157-15174.
15. Willis M. C.; McNally, S. J.; Beswick, P. J. Chelation-Controlled Intermolecular Hydroacylation: Direct Addition of Alkyl Aldehydes to Functionalized Alkenes. *Angew. Chem. Int. Ed.* **2004**, 43, 340-343.
16. Chaplin, A. B.; Hooper, J. F.; Weller, A. S.; Willis, M. C. Intermolecular Hydroacylation: High Activity Rhodium Catalysts Containing Small-Bite-Angle Diphosphine Ligands. *J. Am. Chem. Soc.* **2012**, 134, 4885-4897.
17. González-Rodríguez, C.; Willis, M. C. Rhodium-catalyzed enantioselective intermolecular hydroacylation reactions. *Pure Appl. Chem.* **2011**, 83, 577-585.
18. Jugé, S.; Stephan, M.; Laffitte, J. A.; Genêt, J. P. Efficient Asymmetric Synthesis of Opically Pure Tertiary Mono and Diphosphine Ligands. *Tetrahedron Lett.* **1990**, 31, 6357-6360.

19. Eusamio, J.; M. Medina, Y.; Córdoba, J. C.; Vidal-Ferran, A.; Sainz, D.; Gutiérrez, A.; Font-Bardia, M.; Grabulosa, A. Rhodium and Ruthenium Complexes of Methylene-Bridged, P-Stereogenic, Unsymmetrical Diphosphanes. *Dalton Trans.* **2023**, 52, 2424-2439.
20. Córdoba, J. C.; Vidal-Ferran, A.; Font-Bardia, M.; Grabulosa, A. Palladium Complexes of Methylene-Bridged *P*-Stereogenic, Unsymmetrical Diphosphines. *Organometallics* **2020**, 39, 2511-2525.
21. Gridnev, I. D.; Yasutake, M.; Higashi, N.; Imamoto, T. Asymmetric Hydrogenation of Enamides with Rh-BisP* and Rh-MiniPHOS Catalysts. Scope, Limitations and Mechanism. *J. Am. Chem. Soc.* **2001**, 123, 5268-5276.
22. Malkina, O. L.; Hierso, J.C.; Malkin, V. G. "Distinguishing Through-Space" from "Through-Bonds" Contribution in Indirect Nuclear Spin–Spin Coupling: General Approaches Applied to Complex J_{PP} and J_{PSe} Scalar Couplings. *J. Am. Chem. Soc.* **2022**, 144, 10768-10784.
23. Matsusaka, Y.; Shitaya, S.; Nomura, K.; Inagaki, A. Synthesis of Mono-, Di-, and Trinuclear Rhodium Diphosphine Complexes Containing Light-Harvesting Fluorene Backbones. *Inorg. Chem.* **2017**, 56, 1027-1030.
24. Preetz, A.; Baumann, W.; Fischer, C.; Drexler, H.; Schmidt, T.; Thede, R.; Heller, D. Asymmetric Hydrogenation, Dimerization of Solvate Complexes: Synthesis and Characterization of Dimeric $[Rh(DIPAMP)]_2^{2+}$, a Valuable Catalyst Precursor. *Organometallics* **2009**, 28, 3673-3677.
25. Faller, J. W.; Friss, T.; Parr, J. Hemilability and regioselectivity in palladium and platinum complexes of dppm(*E*) [*E* = O, S, Se] ligands. *J. Organomet. Chem.* **2010**, 24, 2644-2650.
26. Hoge, G.; Wu, H.; Kissel, W. S.; Pflum, D. A.; Greene, D. J.; Bao, J. Highly Selective Asymmetric Hydrogenation Using a Three Hindered Quadrant Bisphosphine Rhodium Catalyst. *J. Am. Chem. Soc.* **2004**, 126, 5966-5967.
27. Pernik, I.; Hooper, J. F.; Chaplin, A. B.; Weller, A. S.; Willis, M. C. Exploring Small Bite-Angle Ligands for the Rhodium-Catalyzed Intermolecular Hydroacylation of *β*-S-Substituted Aldehydes with 1-Octene and 1-Octyne. *ACS Catal.* **2012**, 2, 2779-2786.
28. Fairlie, P.; Bosnich, B. Homogeneous catalysis. Conversion of 4-pentenals to cyclopentanones by efficient rhodium-catalyzed hydroacylation. *Organometallics* **1988**, 7, 936-945.
29. Mann, F. G.; Tong, B. P.; Wystrach V. P. The abnormal hydrolysis of certain β-(diarylphosphino)-propionic esters. Part II. *J. Chem. Soc.* **1963**, 0, 1155-1166.
30. Douglas, T. M.; Brayshaw, S. K.; Dallanegra, R.; Kociok-Köhn, G.; Macgregor, S. A.; Moxham, G. L.; Weller, A. S.; Wondimagegn, T.; Vadivelu, P. Intramolecular Alkyl Phosphine Dehydrogenation in Cationic Rhodium Complexes of Tris(cyclopentylphosphine). *Chem. Eur. J.* **2008**, 14, 1004-1022.
31. Grellier, M.; Sabo-Etienne, S. Dehydrogenation processes via C-H activation within alkylphosphines. *Chem. Commun.* **2011**, 48, 34-42.
32. Jover, J.; Cirera, J. Computational assessment on the Tolman cone angles for P-ligands. *Dalton Trans.* **2019**, 48, 15036-15048.

12. ACRONYMS

cod: 1,5-Cyclooctadiene

COSY: Correlated Spectroscopy

DCM: Dichloromethane

dcPAMP: dichickenPAMP

HRMS: High Resolution Mass Spectroscopy

HSQC: Heteronuclear Single-Quantum Correlation

IR: Infrared spectroscopy

nbd: Norbornadiene

NMR: Nuclear Magnetic Resonance

NOESY: Nuclear Overhauser Effect Spectroscopy

PAMP: (*o*-anysyl)(methyl)phenylphosphane

TCFP: Trichickenfootphos

THF: Tetrahydrofuran

XRD: X-Ray Diffraction